RSC Advances

ROYAL SOCIETY OF CHEMISTRY

www.rsc.org/advances

Developing High-efficiency π Conjugated Polymer Semiconductor for Photocatalytic Degradation of Dyes under Visible Light Irradiation

Sheng Chu, [a] Cuicui Wang, [a] Yu Yang, [a] Ying Wang,*[, a, b] Zhigang Zou,*[, a, b]

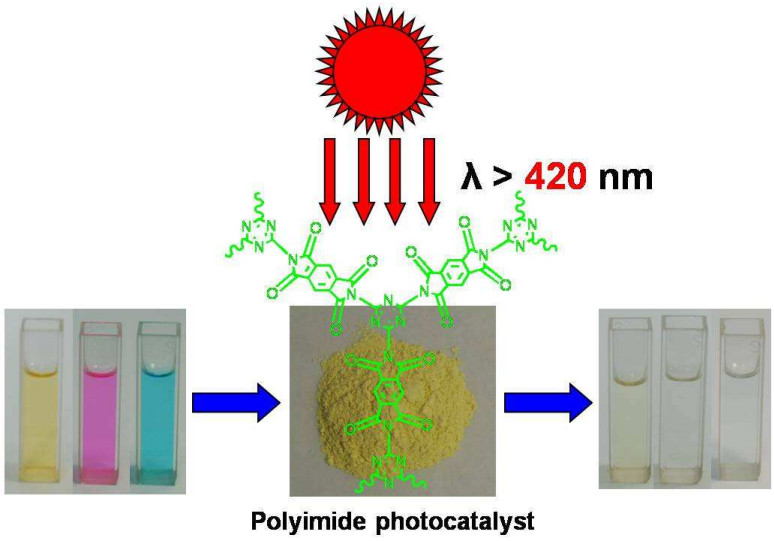

π-conjugated polymer with a good coplanar backbone conformation exhibits high activity for degradation of pollutant under visible irradiation.

Cite this: DOI: 10.1039/c0xx00000x

ARTICLE TYPE

www.rsc.org/xxxxxx

Developing High-efficiency π Conjugated Polymer Semiconductor for Photocatalytic Degradation of Dyes under Visible Light Irradiation

Sheng Chu, [a] Cuicui Wang, [a] Yu Yang, [a] Ying Wang,*[ab] Zhigang Zou,*[ab]

Received (in XXX, XXX) Xth XXXXXXXXX 20XX, Accepted Xth XXXXXXXXX 20XX

DOI: 10.1039/b000000x

Abstract: In this study, a series of conjugated polyimide (PI) photocatalysts were prepared via a facile thermal condensation of melamine and various aromatic dianhydride monomers. The samples were characterized by Fourier transform infrared spectroscopy, elemental analysis, X-ray powder diffraction and UV-Vis diffuse reflectance spectroscopy. All samples showed a well-developed polyimide structure and strong visible-light absorption. The electronic band structures of PI were simulated by density functional theory calculations. Photocatalytic results showed that the PI with a best coplanar conformation in the backbone and strongest photooxidative capability exhibited the highest activity for methyl orange (MO) degradation. In addition, it displayed an excellent stability during four cycles of photocatalytic testing. Photocatalytic mechanism study indicated that photogenerated holes rather than electrons play a crucial role on the photodegradation of MO. Moreover, the participation of reactive oxygen species such as OH•, $O_2^{\bullet-}$ and $^1O_2$ was examined by adding corresponding scavengers. However, only $^1O_2$ was identified as the active species involved in the MO degradation. This work represents the great potential of metal-free PI photocatalyst as sustainable, efficient and low-cost material for environmental remediation and solar energy conversion.

Introduction

Heterogeneous photocatalysis has attracted tremendous attention for their promising potential to settle intractable energy and environment issues. Nowadays, water environments are threatened by a variety of hazardous chemical substances derived from industrial and/or domestic effluents, including dyes and other organic compounds. Among various available methods for the removal of organic pollutants, photocatalysis is one of the most promising technologies because it is performed at ambient conditions by utilizing sunlight as energy source [1]. Over the past decade, extensive studies have been made to seek innovative photocatalyst working with visible-light irradiation to efficiently utilize the solar energy. The explorations up to now have been dominated by metal-containing inorganic materials including TiO_2-based [2-3] and non-TiO_2-based systems, whereby Ga, In, Nb, Ta, W and Bi are the main metal constituents [4]. Despite spectacular advances in environmental photocatalysis, the search for cost-effective and sustainable photocatalysts active in the visible light region is of particular interest for the large-scale utilization of solar light. Organic photocatalysts in this context hold great promise owing to their abundant sources, low-cost fabrication and strong absorption in the visible region [5].

Organic π conjugated polymer has semiconducting properties due to the overlap of their π bonds. The delocalized π electron system can absorb light to generate charge carriers for subsequent photochemical reactions. However, the cheap and facile reaction protocol for the synthesis of organic semiconductor is always counterbalanced by their limited catalytic activity and stability. For example, the first polymeric photocatalyst poly(p-phenylene) (PPP) exhibited low activity in the visible region and decomposed gradually under irradiation [6]. Recently, it was reported that graphitic carbon nitride (g-C_3N_4) could function as a stable polymeric photocatalyst for hydrogen/oxygen evolution from water and organic pollutants degradation under visible light irradiation [7-8], which inspiring the exploration of novel visible light driven metal-free photocatalyst. Very recently, we presented a new organic photocatalyst based on crystalline polyimide (PI) network for H_2 production from water [9-10]. The PI was synthesized via direct thermal condensation of commercial available melamine (MA) and pyromellitic dianhydride (PMDA) monomers at a mild temperature. The synthetic process is cost-effective and environmentally-friendly with only water released as a by-product. This work opens a new window for the synthesis of π conjugated polymer photocatalyst. However, the underlying structure-property relationship of PI is more appealing in material synthesis science and material engineering. In this work, we synthesized a series of PI polymer photocatalysts by tuning the chemical structure of dianhydride moiety and evaluated their photocatalytic dye degradation activity under visible light irradiation. A judicious choice of the comonomer building blocks for constructing the network of a high-efficiency PI polymer photocatalyst was explored. Moreover, the photocatalytic mechanism of dye degradation on PI was also investigated.

Experimental

Sample preparation

Melamine (MA) was purchased from Shanghai Lingfeng Chemical Reagent Co., Ltd. All dianhydride monomers were purchased from TCI Shanghai Chemical Reagent Co., Ltd.

Three kinds of PI photocatalysts were synthesized in the following procedure: MA and dianhydride [pyromellitic dianhydride (PMDA); 3,3',4,4'-biphenyltetracarboxylic dianhydride (BPDA) and 3,3',4,4'-benzophenonetetracarboxylic dianhydride (BTDA)] with equal molar ratio (10 mmol) were mixed uniformly in an agate mortar, respectively. Then the mixture was put into a porcelain crucible with a cover and heated at 7 °C /min up to 325 °C, 350 °C and 300 °C for 4 h, respectively. The resultant yellow solid was ground into powder and washed with water at 50 °C to remove any residual monomers if exist. Finally, the solid was filtered and dried at 100 °C overnight. The sample was denoted as PI-1, PI-2 and PI-3 corresponding to the used dianhydride monomers PMDA, BPDA and BTDA. The product yield was 95%, 97% and 98%, respectively. It is worth noting that the different polymerization temperatures selected for the three PI samples are ascribed to the different melting points of dianhydride monomers (286 °C, 302 °C and 226 °C for PMDA, BPDA and BTDA, respectively). According to our previous report [10], there is an optimum temperature that slightly higher than the melting point of dianhydride monomers to achieve desired condensation degree and photocatalytic property. g-C_3N_4 was prepared by heating 5 g of melamine at 550 °C for 4 h according to our previous study [11].

Characterization

Fourier transform infrared spectroscopy (FTIR) spectra were recorded on a Nicolet NEXUS870 spectrometer. Elemental analysis was determined by Elementar vario EL analyzer. X-ray diffraction (XRD) measurements were performed on a Rigaku Ultima III X-ray diffractometer using CuKα radiation. UV-Vis spectra were collected by Shimadzu UV-2550 spectrometer. Specific surface area was measured using Micromeritics Tristar-3000 equipment.

Photocatalytic dye degradation

A 300 W Xenon arc lamp was used as the light source, and visible light irradiation was realized by attaching a 420 nm cutoff filter. The reactor vessel was kept at 25 °C using circulated water. 0.2 g catalyst was added to 100 mL dye solution (4 mg · L^{-1}). Prior to irradiation, the dye solution over the catalyst was stirred in the dark for 1 h to reach the sorption equilibrium. During the irradiation, about 4 mL liquid was taken from the reaction cell at regular time intervals. The dye solution was analyzed by UV-Vis spectrometer (Shimadzu UV-1750). The concentration of methyl orange (MO), Rhodamine B (RhB) and Methylene Blue (MB) are referred to the characteristic absorption at 464, 554 and 665 nm, respectively.

In the N_2-purging experiment, the reaction setup was vacuum-treated and then purged with high-purity N_2 (99.999%). The same process was repeated several times to eliminate O_2 completely. The N_2 gas was purged at a rate of 50 mL/min during the photodegradation.

Theoretical calculation

All calculations were performed with Gaussian 03 program. Optimized organic models were constructed with Gview program based on the B3LYP/6-31g-optimized results. The highest occupied molecular orbital (HOMO) and lowest unoccupied molecular orbital (LUMO) were obtained with Gview program on the basis of the B3LYP/6-31g-optimized results.

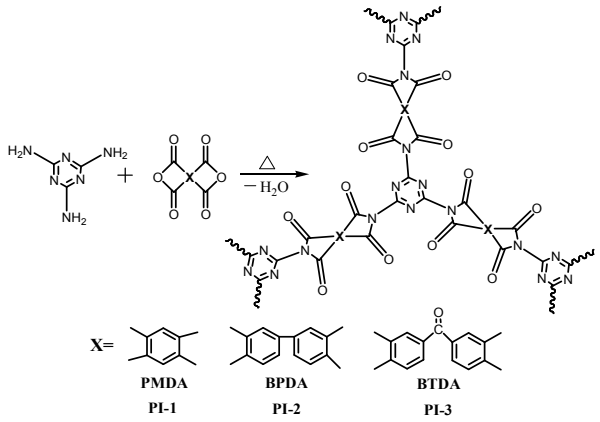

Scheme 1. Reaction scheme for the synthesis of PI-1, PI-2 and PI-3.

Results and Discussion

Three PI networks were synthesized via direct thermal condensation of MA and dianhydride monomers (PMDA, BPDA and BTDA), as depicted in Scheme 1. The formation of polyimide structure in the three PI products is verified by the combination of FTIR and elemental analysis. Fig. 1 shows the FTIR spectra of PI prepared from different dianhydride monomers. All the three samples display the characteristic absorption bands of polyimide. The three bands around 1775, 1722 and 725 cm^{-1} are assigned to the asymmetric stretching, symmetric stretching and bending vibration of C=O in the five-membered imide rings, respectively [9-11]. The band around 1365 cm^{-1} is assigned to the stretching vibration of C-N-C in the imide rings [10, 11]. In addition, for PI-3, it is observed a characteristic band at 1665 cm^{-1} belonging to the stretching vibration of C=O in benzophenone groups [12], suggesting the chemical structure of dianhydride moiety remains intact during the thermal condensation. To further verify the chemical structure of PI products, elemental analysis is conducted, as shown in Table 1. For all PI samples, the experimental results are close to the calculated values, indicating the occurrence of imidization reactions between

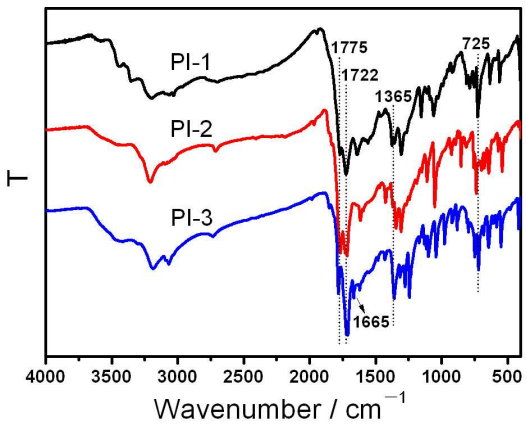

Fig. 1 FTIR spectra of PI-1, PI-2 and PI-3.

Table 1. Elemental analysis and theoretical results of PI-1, PI-2 and PI-3.

Samples	C	H	N	O
PI-1	49.52	2.20	28.70	19.58
PI-1 ($C_{13}H_4N_6O_4$) [a]	50.66	1.31	27.27	20.76
PI-2	59.25	2.21	22.05	16.49
PI-2 ($C_{19}H_8N_6O_4$) [a]	59.38	2.10	21.87	16.65
PI-3	58.10	2.24	20.51	19.15
PI-3 ($C_{20}H_8N_6O_5$) [a]	58.26	1.96	20.38	19.40

[a] Calculated from the imidization reaction in Scheme 1.

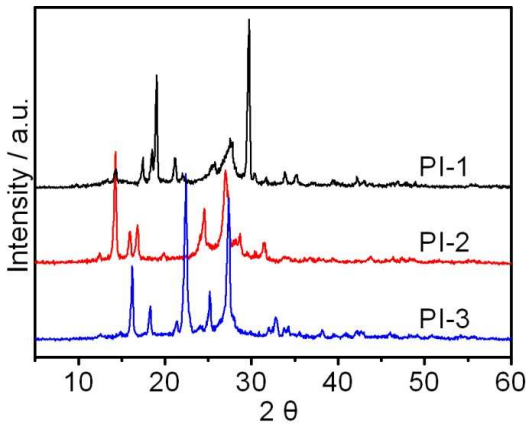

Fig. 2 XRD patterns of PI-1, PI-2 and PI-3.

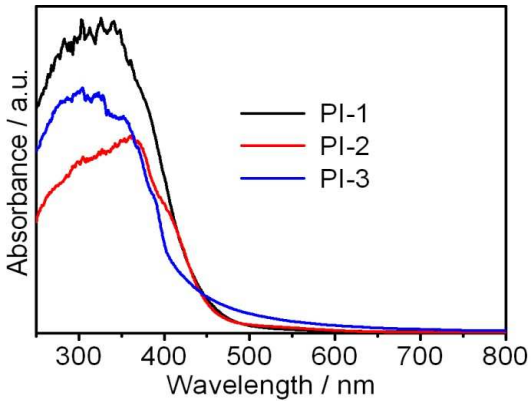

Fig. 3 UV-Vis absorption spectra of PI-1, PI-2 and PI-3.

MA and PMDA/BPDA/BTDA. The higher carbon content in PI-2 and PI-3 than that in PI-1 is ascribed to the relatively higher content of carbon in BPDA and BTDA than that in PMDA. Similarly, PI-3 shows a higher oxygen content than PI-2 due to the increase of one carbonyl group in the dianhydride monomer.

The crystallinity of the three PI samples is characterized by XRD, as shown in Fig. 2. The several apparent peaks in the range of 10-30° clearly demonstrate the high degree of crystallinity in all samples, which is ascribed to the typical melt polymerization process [9]. The highly ordered packing of polymer chains is resulted from the strong π-stacking between the conjugated core units. In addition, the XRD peaks of the three PI samples are

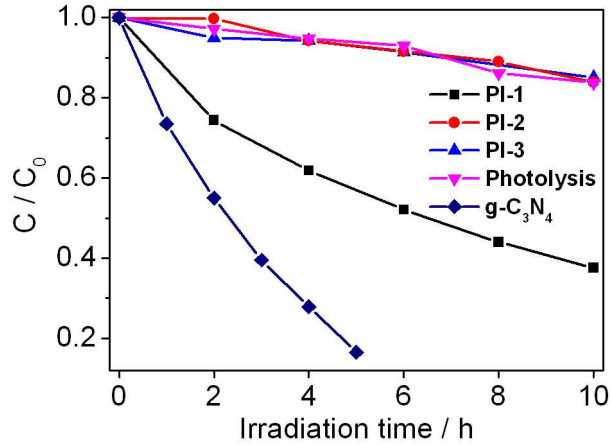

Fig. 4 Time course of degradation of MO in the presence PI-1, PI-2, PI-3 and g-C_3N_4 under visible light irradiation ($\lambda > 420$ nm).

dramatically different, implying that the chain orientation is greatly affected by the dianhydride moiety.

Fig. 3 shows the UV-Vis absorption spectra of PI-1, PI-2 and PI-3. All the three samples exhibit obvious light absorption in the visible region, which is consistent with their yellowish color. PI-1 and PI-2 show similar visible-light absorption, with bandgaps estimated to be 2.7 eV from the intercept on the wavelength axis for a tangent line drawn. Compared with PI-1 and PI-2, PI-3 displays tale absorption up to 700 nm. Because all PI samples have the ability to respond to visible-light, we expect that these materials will present visible-light photocatalytic activity.

To evaluate the photocatalytic activity of the PI samples, we examined the decomposition of MO dye in aqueous solution under visible light irradiation, as shown in Fig. 4. It is found that the photocatalytic performance of PI greatly depends on the building block of dianhydride moiety. Among the three samples, only PI-1 shows distinct photocatalytic activity for MO degradation. Both PI-2 and PI-3 exhibits negligible activity since the control experiment of photolysis (without photocatalyst) shows a comparative degradation performance. As a reference, g-C_3N_4, a state-of-the-art polymer photocatalyst, was also tested under the same reaction conditions. It is found that the photocatalytic activity of PI-1 is about half that of g-C_3N_4. But considering the surface area of PI-1 (5.1 $m^2\ g^{-1}$) is only half that of g-C_3N_4 (10 $m^2\ g^{-1}$), the specific activity of PI-1 is comparable to that of g-C_3N_4, indicating the excellent photocatalytic behavior of PI.

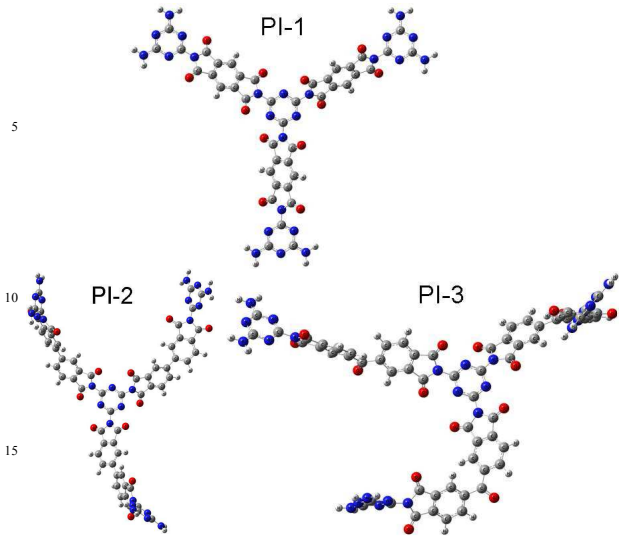

Fig. 5 Optimized PI-1, PI-2 and PI-3 models calculated by B3LYP /6-31g method. The carbon atoms are grey, nitrogen atoms are blue, hydrogen atoms are white and oxygen atoms are red.

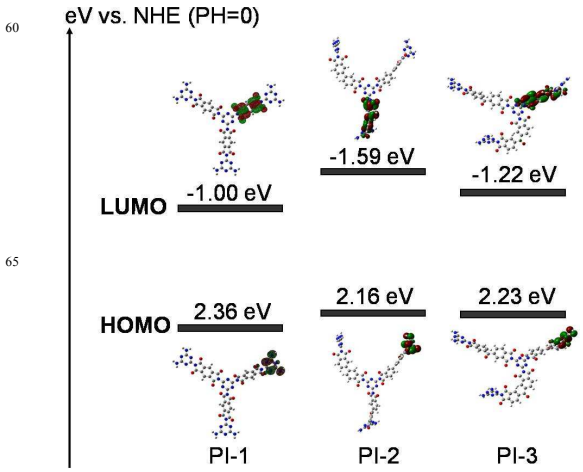

Fig. 6 DFT calculated HOMO and LUMO energy levels of optimized PI-1, PI-2 and PI-3 models.

Moreover, considering the great variety of amine and anhydride building blocks, further structural optimization of the polyimide network can be expected to improve the efficiency in the future.

It is interesting to find that PI-1 displays an entirely different behavior for MO degradation with PI-2 and PI-3, although they have similar optical absorption and surface area (5.1, 4.9 and 6.0 $m^2 g^{-1}$ for PI-1, PI-2 and PI-3, respectively). To gain some deep understanding for the structure-property relationship, density functional theory (DFT) calculations were performed to investigate the optimized geometry and electronic structure of PI models. Fig. 5 shows optimized models of PI clusters based on DFT simulation. Compared with PI-1, the backbone chains of PI-2 and PI-3 have a larger distortion out of coplanarity. It was reported that the charge mobility of polymer semiconductor along the main chains decreased significantly when the deviation degree from backbone planarity increased [13]. So we propose that the charge mobility of PI-1 is much higher than those of twisted PI-2 and PI-3, which leads to the distinctive photocatalytic behavior. The low photocatalytic activities of PI-2 and PI-3 are supposed to be mainly ascribed to the inefficient transport of charge carriers.

It is well known that the electronic band structure of a semiconductor photocatalyst greatly influences its photocatalytic performance. To clarify if there is any correlation between them, DFT calculations were also performed. Fig. 6 shows HOMO and LUMO energy levels of optimized PI models calculated by DFT methods. Both the HOMO and LUMO energy levels of PI-1 are lower than those of PI-2 and PI-3. Because the HOMO and LUMO in a cluster are the counterparts of the valence band (VB) and conduction band (CB) in the material [14]. It is inferred that PI-1 has a higher photooxidation capability but lower photoreduction ability compared to PI-2 and PI-3. In the latter part of this work, the mechanism study of active species shows that the photogenerated holes play a more important role than photoexcited electrons in MO degradation. So we reason that the strong photooxidative capability of PI-1 may also partly contribute to its high photocatalytic activity.

To confirm the MO degradation reaction of PI-1 is driven by light, wavelength dependence of MO degradation rate is obtained by means of kinetic analysis using different cut-off filters, as shown in Fig. 7. It is seen that the degradation process follows a pseudo first-order kinetics equation $\ln(C/C_t) = kt$, where k is the apparent rate constant of the degradation. The degradation rate of MO is in good agreement with the optical absorption of PI-1, indicating the catalytic reaction is really driven by light. This is further verified by a control experiment shown that no degradation takes place in the dark.

The durability of a photocatalyst is important to its application, thus we also investigate the stability of PI-1 for MO degradation, as shown in Fig. 8. It is found that PI-1 reveals an excellent stability during the photocatalysis process, which is contrary to many other reported organic photocatalysts [6, 15-17]. The catalytic activity does not display any decrease after four consecutive runs over a period of 40 h. In addition, the chemical structure of the catalyst is virtually identical to that before the photochemical reaction as confirmed by FTIR and XRD analysis (Fig. 9). The excellent stability of PI-1 is considered to be ascribed to its rigid branch unit and highly cross-linked nature, which has also been proved a great advantage for long-time operation in a recently reported poly(azomethine) photocatalyst [18]. For other dye pollutants such as RhB and MB, PI-1 still exhibits excellent photocatalytic activity under visible light irradiation, with most of dye degraded in 5 h (Fig. 10). This indicates that PI-1 can photodegrade various dye pollutants efficiently. During the photodegradation of RhB and MB, it is also noticed that there are obvious hypsochromic shifts of the maximum absorption peak. After an irradiation time of 5 h, the major absorption band shifts from 554 to 501 nm for RhB, and from 665 to 611 nm for MB. These wavelength shifts are caused by deethylation and demethylation of RhB and MB, respectively [19-21]. Reactive oxygen species (ROS) produced during the photocatalytic process attack the N-ethyl or N-methyl groups

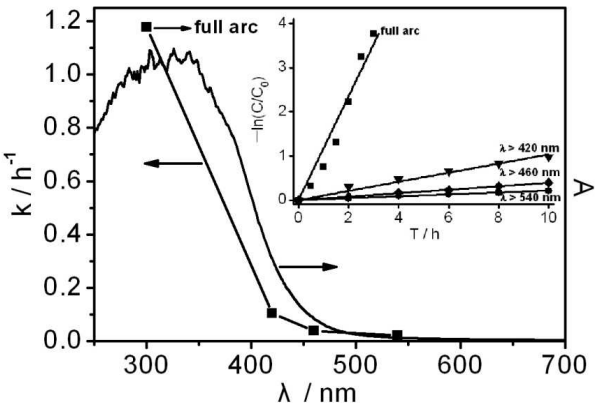

Fig. 7 Wavelength dependence of MO degradation rate (k) over PI-1. Inset: Kinetic curves of MO degradation over PI-1 using different cut-off filters.

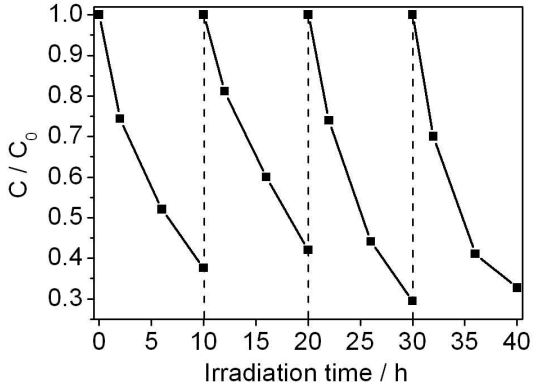

Fig. 8 Degradation of MO over PI-1 during repeated experiments under visible light irradiation (λ > 420 nm).

of RhB and MB to form a series of de-ethylated or demethylated intermediates in a stepwise manner, leading to the gradual peak wavelength shifts toward the blue region. During the photodegradation of RhB and MB, photoreactions of de-alkylation and cleavage of chromophore ring structure occur simultaneous, resulting in the decrease of intensity of the maximum absorption peak with a concomitant blue shift.

The efficient and stable photocatalytic activity of PI-1 motivates us to further investigate the underlying mechanism for MO degradation. To determine what species are involved in the photoreaction, N_2 purging and scavengers adding experiments are performed (Fig. 11). Full arc light (λ > 300 nm) is used as the light source to better observe the variation of degradation rate. A control experiment shows that the photolysis of MO under full arc light is slight, which is consistent with reported result that MO is a stable organic contaminant under UV-Vis irradiation if there is no photocatalyst involved [22]. After introducing PI-1 photocatalyst, MO is decomposed completely after 3 h light irradiation. Under N_2 atmosphere, however, only about 70% MO is degraded in 3 h, suggesting that molecular oxygen is participated in part of the catalytic process. Singlet oxygen ($^1O_2$), superoxide radical anion ($O_2^{\bullet-}$) and hydroxyl radical (OH•) are reported to be the three most common ROS involved in organic pollutant degradation [5, 23-24]. It is shown that $^1O_2$ plays an important role in the photoreaction since the MO degradation rate

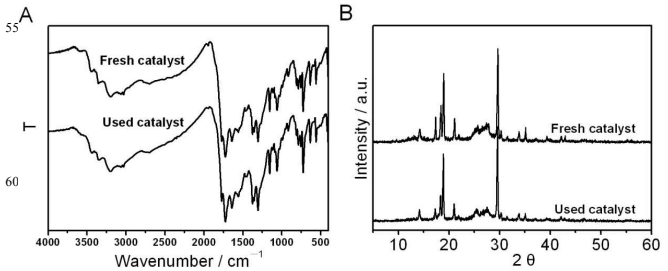

Fig. 9 (A) FTIR spectra and (B) XRD patterns of PI-1 sample before and after photodegradation of MO under visible light irradiation (λ > 420 nm).

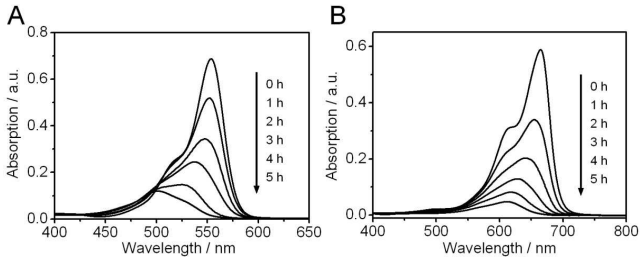

Fig. 10 UV-Vis spectra of (A) RhB and (B) MB solution as a function of irradiation time in the presence of PI-1 under visible light irradiation (λ > 420 nm).

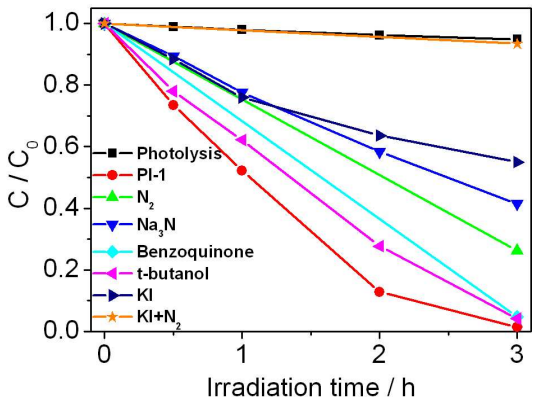

Fig. 11 Time course of degradation of MO under full arc light (λ > 300 nm) without catalyst, with PI-1, with PI-1 in an N_2-purged system, in the presence of PI-1 with various scavengers: 10 mM NaN_3; 0.1 mM benzoquinone; 10 mM t-butanol; 10 mM KI, 10 mM KI in an N_2-purged system.

is inhibited after introducing NaN_3 as $^1O_2$ scavengers. In contrast, by adding benzoquinone and t-butanol as scavengers for $O_2^{\bullet-}$ and OH• respectively, there is no obvious change of MO degradation, suggesting $O_2^{\bullet-}$ and OH• are not active species involved in MO degradation. Yet it is deduced that there are some other active species besides $^1O_2$ since most of MO dye is still decomposed in the absence of O_2. It is found that there is a decrease of about 60% in the rate of MO degradation after the introduction of KI as hole scavenger [23-24]. So, we infer that MO degradation is the cooperative contribution of $^1O_2$ and photogenerated holes by interacts with the substrate MO to the corresponding oxidation products. The proposed mechanism is further verified by the full inhibition of MO degradation when both KI and N_2 are introduced into the system.

Conclusions

In summary, we have prepared a series of PI via a facile thermal condensation of melamine and various aromatic dianhydride monomers. The copolymer nature of this organocatalyst allows flexible organic protocol to modify its chemical structure and catalytic property. It is found that the PI with a better coplanar conformation in the backbone and stronger photooxidative capability exhibits higher activity for MO photodegradation. In addition, PI reveals an excellent stability during the photocatalysis process. Both $^1O_2$ and photogenerated holes are reactive species contributed for the MO degradation. The distinct advantages of cheap and sustainable, together with high stability and efficiency, make this polyimide material particularly interesting for environmental remediation and solar energy conversion.

ACKNOWLEDGMENT

This work was financially supported by NSFC (21273111, 21273106, 51272101), the National Basic Research Program of China (973 Program, 2013CB632404) and the Jiangsu Provincial Natural Science Foundation (No.BK20130053); The authors thank Analysis Center and High Performance Computing Center of Nanjing University for the characterization and theoretical calculation of materials.

Notes and references

[a] Eco-materials and Renewable Energy Research Center (ERERC), School of Chemistry and Chemical Engineering, National Laboratory of Solid State Microstructures, Kunshan Innovation Institute of Nanjing University, Nanjing 210093, China. E-mail: wangy@nju.edu.cn
[b] Kunshan Innovation Institute of Nanjing University, Kunshan 215300, P. R. China

1 M. R. Hoffmann, S. T. Martin, W. Choi and D.W. Bahnemann, *Chem. Rev.,* 1995, **95**, 69.
2 M. Pelaez, N. T. Nolan, S. C. Pillai, M. K. Seery, P. Falaras and A. G. Kontos, P.S.M. Dunlop, J. W.J. Hamilton, J. A. Byrne, K. O'Shea, M. H. Entezari, D. D. Dionysiou, *Appl. Catal. B*, 2012, **125**, 331.
3 M. Xue, L. Huang, J. Q. Wang, Y. Wang, L. Gao, J. H. Zhu and Z. G. Zou, *Nanotechnology,* 2008, **19,** 185604.
4 M. D. Hernandez-Alonso, F. Fresno, S. Suarez and J. M. Coronado, *Energy Environ. Sci.,* 2009, **2**, 1231.
5 M. L. Marin, L. S. Juanes, A. Arques, A. M. Amat and M. A. Miranda, *Chem. Rev.*, 2012, **112**, 1710.
6 S.Yanagida, A. Kabumoto, K. Mizumoto, C. Pac and K. Yoshino, *J. Chem., Soc., Chem. Commun.,* 1985, **8**, 474.
7 X. C. Wang, K. Maeda, A. Thomas, K. Takanabe, G. Xin, J. M. Carlsson, K. Domen and M. Antonietti, *Nat. Mater.,* 2009, **8**, 76.
8 S. C. Yan, Z. S. Li and Z. G. Zou, *Langmuir,* 2009, **25**, 10397.
9 S. Chu, Y. Wang, Y. Guo, P. Zhou, H. Yu, L. L. Luo, F. Kong and Z. G. Zou, *J. Mater. Chem.,* 2012, **22**, 15519.
10 S. Chu, Y. Wang, C. C. Wang, J. C. Yang and Z. G. Zou, *Int. J. Hydrogen Energy,* 2013, **38**, 10768.
11 S. Chu, Y. Wang, Y. Guo, J. Y. Feng, C. C. Wang, W. J. Luo, X.X. Fan and Z.G. Zou, *ACS Catal.,* 2013, **3**, 912.
12 A. C. T. Cursino, F. S. Lisboa, A. S. Pyrrho, V. P. Sousa and F. Wypych, *J. Colloid Interface Sci.,* 2013, **397**, 88.
13 Y. K. Lan and C. I. Huang, *J. Phys. Chem. B,* 2008, **112**, 14857.
14 Y. Guo, F. Kong, S. Chu, L. L. Luo, J. C. Yang, Y. Wang and Z. G. Zou, *RSC Adv.,* 2012, **2,** 5585.
15 H. Y. Kim, T. G. Bjorklund, S.H. Lim and C. J. Bardeen, *Langmuir,* 2003, **19**, 3941.
16 T. F. Yeh, J. M. Syu, C. Cheng, T. H. Chang and H. Teng, *Adv. Funct. Mater.,*2010, **20**, 2255.
17 H.Yan and Y. Huang, *Chem. Commun.,* 2011, **47,** 4168.
18 M. G. Schwab, M. Hamburger, X. L. Feng, J. Shu, H. W. Spiess, X. C.Wang, M. Antonietti and K. Müllen, *Chem. Commun.,* 2010, **46**, 8932.
19 T. X. Wu, G. M. Liu and J. C. Zhao, *J. Phys. Chem. B,* 1998, **102,** 5845.
20 Y. J. Cui, Z. X. Ding, P. Liu, M. Antonietti, X. Z. Fu and X. C. Wang, *Phys. Chem. Chem. Phys.,* 2012, **14,** 1455.
21 C. Yogi, K. Kojima, N. Wada, H. Tokumoto, T. Takai, T. Mizoguchi, H. Tamiaki, *Thin Solid Films,* 2008, **516,** 5881.
22 F. Gao, X. Y. Chen, K. B. Yin, S. Dong, Z. F. Ren, F. Yuan, T. Yu, Z. G. Zou and J. M. Liu, *Adv. Mater.,* 2007, **19**, 2889.
23 J. H. Kou, Z. S. Li, Y. P. Yuan, H. T. Zhang, Y. Wang and Z. G. Zou, *Environ. Sci. Technol.,* 2009, **43**, 2919.
24 R. Palominos, J. Freer, M. A. Mondaca and H. D. Mansilla, *J. Photochem. Photobiol. A: Chem.,* 2008, **193**, 139.